*J. Fluid Mech.* (2004), *vol.* 511, *pp.* 217–236.  
DOI: 10.1017/S0022112004009644 Printed in the United Kingdom

# Flow in the negative wake of a Taylor bubble rising in viscoelastic carboxymethylcellulose solutions: particle image velocimetry measurements

By RENATO G. SOUSA[1], S. NOGUEIRA[1, 2], A. M. F. R. PINTO[1], M. L. RIETHMULLER[2] AND J. B. L. M. CAMPOS[1]†

[1]Departamento de Engenharia Química, Centro de Estudos de Fenómenos de Transporte, Faculdade de Engenharia da Universidade do Porto, Rua Dr. Roberto Frias 4200-465 Porto, Portugal

[2]von Karman Institute for Fluid Dynamics, 72 Chaussée de Waterloo, 1640 Rhode-Saint-Genèse, Belgium

(Received 6 May 2003 and in revised form 9 March 2004)

A simultaneous technique employing particle image velocimetry (PIV) and shadowgraphy was used to study vertical slug flow in non-Newtonian fluids. Two aqueous solutions of 0.8 and 1.0 wt% carboxymethylcellulose (CMC) were studied and the flow field around individual Taylor bubbles fully characterized. The rheological fluid properties and pipe dimension yielded Reynolds numbers of 8 and 4 and Deborah numbers of 0.2 and 0.4. A negative wake was found downstream of the Taylor bubbles in both fluids. Below the bubble trailing edge, along the axis region, the fluid flows in the opposite direction to the bubble (negative wake), originating rotational liquid movements in adjacent regions. Even far downward from the bubble, rotational liquid movements are clearly seen and measured. In the 1.0 wt% CMC solution, the bubble trailing edge has the shape of a two-dimensional cusp. This two-dimensional cusp, of small dimensions, is seen in different orientations during the bubble rise-indicating a fast rotational movement. The asymmetrical shape of the trailing edge is responsible for small asymmetries in the flow in the wake region (three-dimensional flow). The asymmetrical shape associated with the rotational movement is responsible for an unsteady flow of small amplitude. In the 0.8 wt% CMC solution, the shape of the trailing edge changes during the bubble rise. An axisymmetric axial oscillation a continuous expansion and contraction of the trailing edge, is the origin of this behaviour. This oscillatory movement is responsible for an unsteady flow of small amplitude in the wake region.

## 1. Introduction

Slug flow is a two-phase flow pattern observed when gas and liquid flow simultaneously in a pipe, over a determined range of flow rates. It is characterized by long bubbles (also called Taylor bubbles or gas slugs) almost filling the pipe cross-section, and liquid flowing around and between the bubbles. This flow regime is found in several industrial processes, such as absorption columns, air-lift reactors, cooling system of nuclear power plants, oil and gas wells and geothermal processes

† Author to whom correspondence should be addressed: jmc@fe.up.pt.

among others. Although the slug regime is sometimes a side effect to be avoided, it is of extreme importance in some chemical processes where it promotes mixing, increasing the reaction rate. In most of the cases, the falling liquid film flowing around the Taylor bubble separates at the rear of the bubble inducing a liquid wake. The velocity of a bubble depends on the flow pattern ahead of its nose (see Moissis & Griffith 1962). When two consecutive bubbles flow in a pipe, the wake of the leading bubble increases the velocity of the trailing one if they are separated by a distance smaller than the minimum stable length (see Taitel, Barnea & Dukler 1980). This increase of velocity leads to the coalescence of the bubbles. Coalescence strongly reduces the mixing process efficiency, once the number of mixing zones decreases. For a better understanding of the coalescence phenomenon it is essential to understand the flow around a single bubble. Several studies have been made in this field, mainly with Newtonian liquids. White & Beardmore (1962) performed experimental and dimensional studies to correlate the individual Taylor bubble velocity with physical and geometric parameters. Campos & Guedes de Carvalho (1988) performed an experimental study to characterize the wake structure for different liquid flow regimes. Pinto & Campos (1996) studied the interaction between two consecutive bubbles and established minimum stable lengths for different operation conditions. Polonsky, Barnea & Shemer (1998), Nogueira *et al.* (2000), van Hout *et al.* (2001) and Bugg & Saad (2002) performed PIV measurements to study the Newtonian liquid flow pattern around individual Taylor bubbles. There are, however, industrial processes where non-Newtonian behaviour is found in some fluids, as is the case of several biological and waste-treatment air-lift reactors and polymer devolatilization processes. Because of the complex liquid rheology, the gas–liquid flow patterns have completely different characteristics, and by consequence different bubble interaction behaviour. Therefore, there is a need to extend the slug flow research towards non-Newtonian liquids. Some studies have been made with small bubbles in non-Newtonian liquids. Bubble velocities and shapes in non-Newtonian liquids have been studied by Astarita & Apuzzo (1965), Leal, Skoog & Acrivos (1971) and Acharya, Mashelkar & Ulbrecht (1977) among others. Hassager (1979) described, for the first time, a negative wake behind small and unconfined bubbles rising in non-Newtonian liquids. Hassager observed (and showed for the first time) a two-dimensional cusp in the trailing edge of these small bubbles. Liu, Liao & Joseph (1995) describe this two-dimensional cusp and review previous studies on this subject. Bubble coalescence in non-Newtonian liquids was studied by Acharya & Ulbrecht (1978), De Kee, Chhabra & Dajan (1990) and Li *et al.* (2001) among others. Funfschilling & Li (2001) used particle image velocimetry (PIV) and birefringence visualization to study the flow of non-Newtonian fluids around small bubbles.

The information about the flow around Taylor bubbles in non-Newtonian liquids is scarce. Carew, Thomas & Johnson (1995) studied the effects of power law rheology and pipe inclination on slug bubble rise velocity. Otten & Fayed (1976) studied the pressure drop and friction drag reduction in two-phase non-Newtonian slug flow. Rosehart, Rhodes & Scott (1975) measured the void fraction, slug velocity and frequency for co-current slug flow of air bubbles in highly viscous non-Newtonian fluids. Terasaka & Tsuge (2003) performed gas hold-up measurements for slug bubbles rising in viscous liquids having a yield stress.

In the present work, a simultaneous PIV and shadowgraphy technique, developed by Lindken & Merzkirch (2001) for bubbly flow and adapted by Nogueira *et al.* (2003) to slug flow, was used to characterize the flow patterns around Taylor bubbles rising in viscoelastic non-Newtonian fluids.

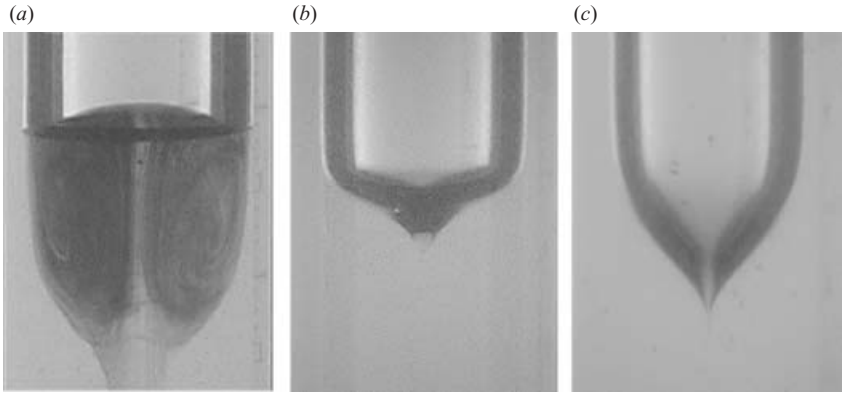


FIGURE 1. Visualization studies with (*a*) 0.4, (*b*) 0.8 and (*c*) 1.0 wt% CMC solutions.

Preliminary visualization studies were performed with solutions of different carboxymethylcellulose (CMC) wt%. The technique applied is described by Campos & Guedes de Carvalho (1988). A coloured CMC solution (inert dye) was placed in the lower part of an acrylic tube with an internal diameter of 32 mm. At the top of this coloured solution, there was a ball valve. With the valve closed, the upper section of the tube was filled with the same CMC solution, but colourless. After the opening of the valve, individual Taylor bubbles were injected at the bottom, and their images rising in the colourless liquid recorded by a fast CCD camera. Figure 1 shows the wake of Taylor bubbles rising in (*a*) 0.4, (*b*) 0.8 and (*c*) 1.0 wt% CMC solutions.

For 0.4 wt%, there is a well-defined portion of liquid (wake) attached to the bottom of the bubble, rising up at the bubble velocity. Inside the wake, there is a toroidal axisymmetrical liquid recirculation similar to that found in Newtonian fluids. For 0.8 and 1.0 wt%, the shape of the trailing edge of the bubble changes drastically, there is no defined wake and no upward liquid transport. The differences found lead the authors to investigate in detail the gas–liquid flow patterns in high CMC concentration solutions, which have viscoelastic behaviour.

## 2. Experiments

### 2.1. *Facility*

The experimental investigation focused on the flow around a single Taylor bubble rising in a vertical column filled with a non-Newtonian viscoelastic stagnant liquid. The experimental facility is schematized in figure 2 and is fully described in Nogueira *et al.* (2000, 2003).

The experiments were performed in an acrylic column 6 m high and of 0.032 m internal diameter. The flow field around the Taylor bubble was obtained applying PIV simultaneously with shadowgraphy. The test section was located near the top of the column, to avoid entrance effects and to assure a stabilized flow. A box with plane faces surrounding the test section (0.5 m $\times$ 0.12 m $\times$ 0.11 m) was filled with the studied liquid in order to minimize optical distortion. The individual Taylor bubbles were injected at the bottom of the column, by manipulating valves A and B. To obtain the Taylor bubble velocity, two laser diodes 0.25 m apart were mounted perpendicularly to the column pointing into two photocells placed in the opposite side

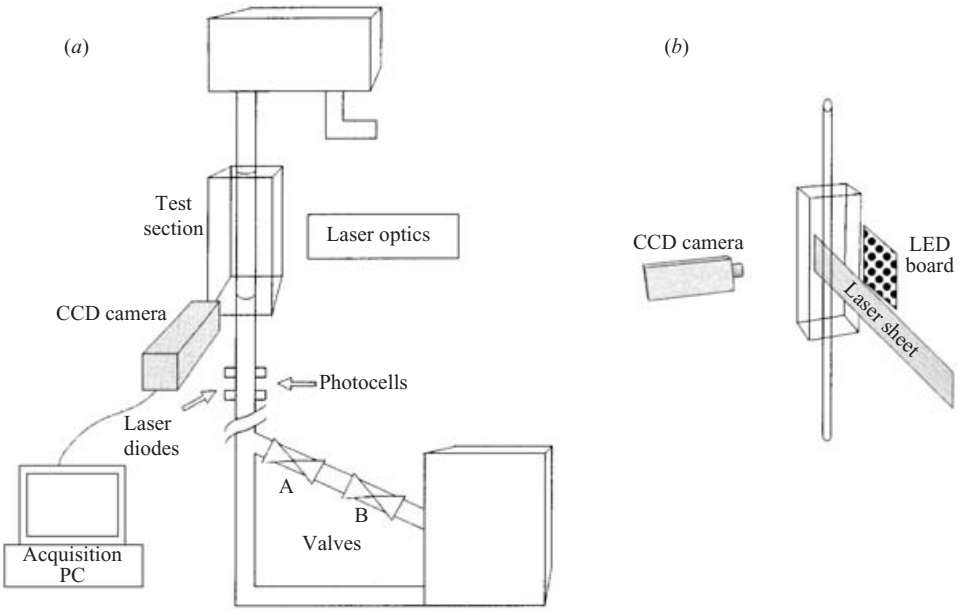


FIGURE 2. Experimental set-up. (*a*) Front view of the experimental test section and instrumentation. (*b*) Side view of the measurement section.

of the column. The PIV instrumentation was composed of a PCO (SensiCam) CCD camera and an acquisition and data processing system. An Nd: YAG laser was used to illuminate the measured plane. An LED array was placed behind the test section with a diffuser paper to obtain the shadow of the Taylor bubble at the same time as the PIV image. Two thermocouples were placed above and below the test section to determine the working temperature and to check a possible temperature gradient along the column. The fluid rheology was determined in an AR 2000 DTA Instruments rheometer.

### 2.2. *Experimental techniques*

The flow field was obtained applying PIV simultaneously with shadowgraphy. Lindken & Merzkirch (2001) presented this simultaneous technique for bubbly flow and Nogueira *et al.* (2003) adapted it for slug flow. The technique is fully described in Nogueira *et al.* (2003) and consists in placing a board of light emitting diodes (LEDs) behind the test section pulsing simultaneously with the laser, so that the CCD camera, with a resolution of 1280 (H) $\times$ 1024 (V) and 4096 grey levels, acquires an image containing both the PIV particles and the shadow of the bubble. A lens of focal length 35 mm was used to obtain the flow field in the nose and wake of the bubble. To obtain a close view of the liquid film around the bubble, a lens of focal length 50 mm and an extension ring of 12 mm were used. The LED array consisted of 350 LEDs emitting light at 650 nm. Fluorescent particles (an orange vinyl pigment, 10 μm of mean size) were used as seeding and emitted light at 590 nm. The particles remained dispersed in the liquid, without floating or depositing after a day's test. An Nd: YAG laser with 400 mJ of pulse power was used to create a vertical laser sheet of about 1 mm thickness containing the axis of the column. The laser wavelength was 532 nm and the pulse duration 2.4 ns. A red filter, opaque below 550 nm, was placed in front of the PCO CCD camera to block the intense green reflections of the

laser and to allow the passage of the light emitted by the fluorescent particles and by the LEDs. The synchronization between camera, laser and LEDs was made with the same signal generator, so that each frame of the camera recorded simultaneously a pulse of the laser and a pulse of the LEDs. The images obtained have different grey levels, corresponding to the seeding particles, background light and bubble shadow, in descending order.

The effects of the optical distortion due to the different indexes of refraction of the CMC solution and test section material were attenuated by the use of a correction box illustrated in figure 2. The use of this box does not completely eliminate the optical distortion, in particular near the tube axis with effects in the radial velocity and radial position. Images of calibration with a very dense scale placed inside the tube show that, at 0.5 mm away from the tube, there is no optical distortion. Between the tube and 0.5 mm, the calibration seems to indicate an extremely low distortion in the radial position, which was impossible to quantify accurately.

The Taylor bubble velocity was determined by dividing the distance between the photocells by the time delay between their signals. The signal yielded by the photocell is proportional to the light received, so when the Taylor bubble is passing between a laser diode and a photocell, the laser beam is deflected and the photocell signal drops abruptly.

## 3. Data processing

The images acquired with the technique used contain both PIV information and the shadow of the bubble. The flow field was obtained using the cross-correlation algorithm WIDIM (window displacement iterative multigrid), developed by Scarano & Riethmuller (1999). A Gaussian interpolation function was used to give an estimate of the location of the correlation peak with subpixel accuracy. In the PIV processing, interrogation windows are displaced according to the first estimation and their size is reduced iteratively. In this work, initial windows had 20 pixels $\times$ 40 pixels and final windows 10 pixels $\times$ 20 pixels. An interrogation areas overlap of 50% was used. Spurious vector identification was used, eliminating vectors with a signal to noise ratio (SNR) less than 1.5 (about 5–7% of the total vectors). These vectors were substituted for interpolated vectors from the neighbours. The average SNR in a processed image was around 10. The time between PIV images varied between 1000 and 2000 μs for the wake and nose regions and 200 and 400 μs for the liquid film around the bubble. As a result of the PIV processing, some vectors appear inside the Taylor bubble owing to erroneous particle images corresponding to reflection and refraction of the light emitted by the particles in the fluid (Nogueira *et al.* 2000). In the PIV images, the gas–liquid interface is not well defined owing to these optical effects. The use of the simultaneous PIV and shadowgraphy technique allows the determination of the exact position of the gas–liquid interface, i.e. the Taylor bubble shape. The definition of the interface was made by sequential image processing. A median filter was applied to the original image (figure 3*a*) to eliminate the seeding particles (figure 3*b*). A background reference image (figure 3*c*) was then subtracted to the filtered image, and the result is the shadow of the bubble (figure 3*d*). The process was completed by defining a grey-level threshold, which puts the image into binary form, and by filling the interior of the Taylor bubble (figure 3*e*). With the bubble shadow, it is then possible to identify the gas–liquid interface and eliminate the erroneous vectors inside the Taylor bubble.

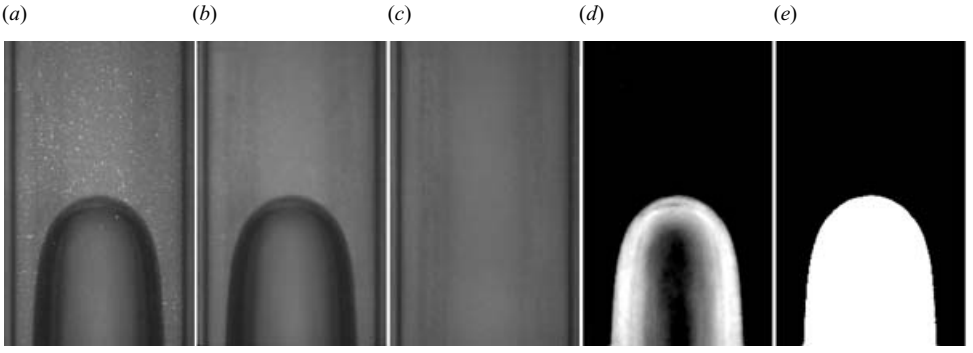


FIGURE 3. Processing of images to obtain a Taylor bubble shadow: (*a*) original image, (*b*) median filtered image, (*c*) background reference image, (*d*) subtraction of *b* and *c*, (*e*) final shadow image.

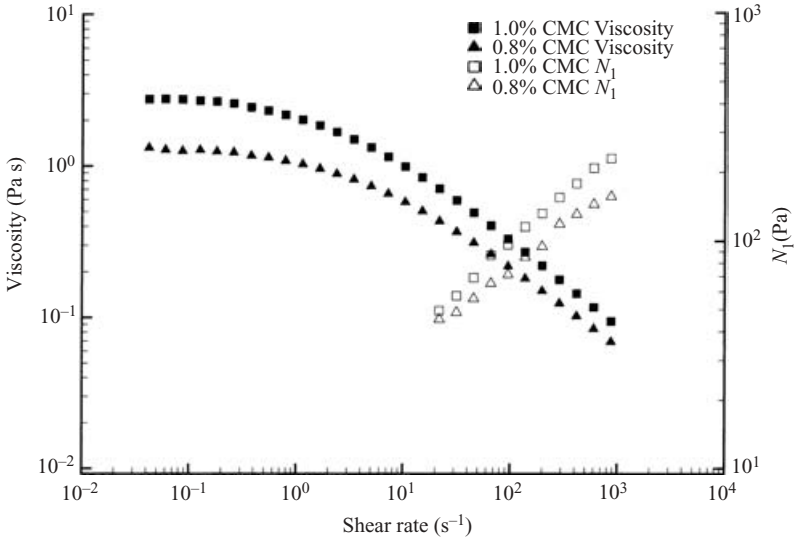


FIGURE 4. Viscosity and first normal stress difference for the 0.8 and 1.0 wt% fluids, measured at the experimental temperature.

## 4. Results

In this work, the flow field around a Taylor bubble rising in two non-Newtonian aqueous solutions of carboxymethylcellulose (CMC) with 0.8 and 1.0 wt% was studied. The molecular mass of the CMC is 300 000 kg kmol$^{-1}$ and the rheological characterization of the fluids was made in an AR 2000 DTA Instruments rheometer. The viscosity and the first normal stress difference dependence on shear rate are presented in figure 4.

In the studied conditions, the Taylor bubbles had a volume around $1 \times 10^{-4}$ m$^3$ and their velocities were $0.182 \pm 0.005$ m s$^{-1}$ for 0.8 wt% and $0.160 \pm 0.005$ m s$^{-1}$ for 1.0 wt%, which correspond to Deborah numbers of 0.2 for 0.8 wt% and 0.4 for 1.0 wt% and Reynolds numbers of 8 and 4, respectively. The Reynolds number ($Re = \rho U_{gb} D/\mu$) was computed using the viscosity at the flow characteristic shear rate ($\dot{\gamma} = U_{gb}/D$), where the subscript *gb* means gas bubble. The Deborah number

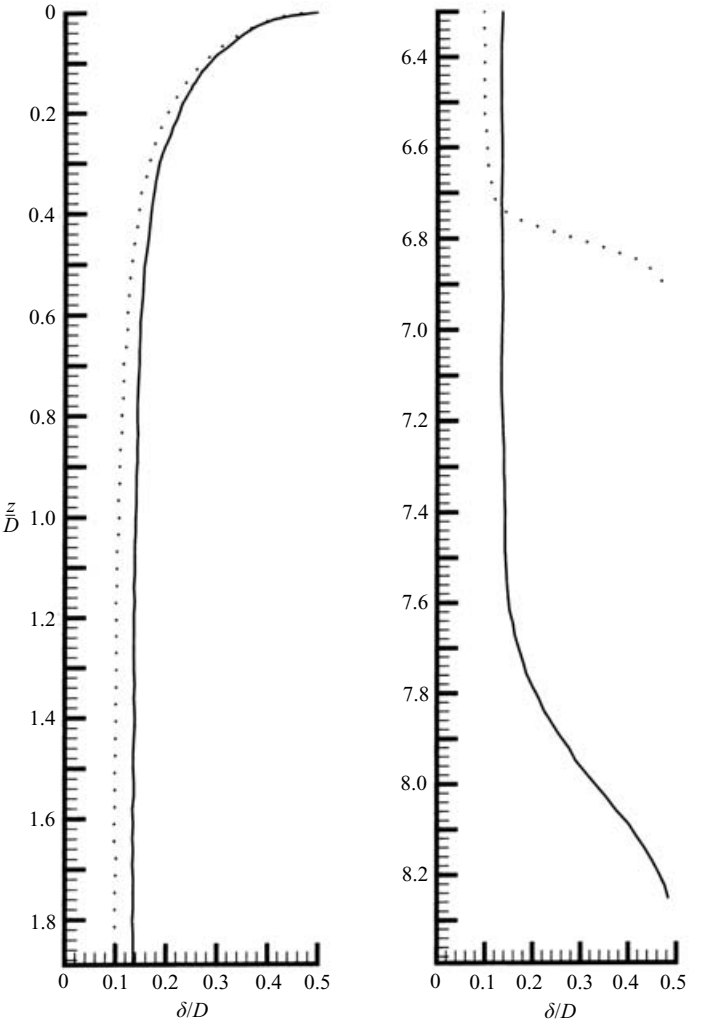


FIGURE 5. Film thickness, $\delta$, versus the distance to bubble nose, $z$. ..., 0.8% CMC; —, 1.0% CMC.

($De = \lambda/\tau$) was computed by dividing the fluid relaxation time ($\lambda$) by a flow characteristic time ($\tau = L_{gb}/U_{gb}$), $U_{gb}$ and $L_{gb}$ being the gas bubble velocity and length, respectively, and $D$ the pipe diameter. The relaxation time used was obtained from adjustment of the viscosity to the Carreau simplified model (4.1), owing to difficulties in direct measurement.

$$\mu = \mu_0(1 + (\lambda\dot{\gamma})^2)^{(n-1)/2}, \tag{4.1}$$

where $\mu_0$ is the viscosity at zero shear rate, $\lambda$ a characteristic time of the fluid, $\dot{\gamma}$ the shear rate and $n$ a dimensionless parameter.

### 4.1. *Taylor bubble shape*

The shape of the Taylor bubble can be accurately obtained from its shadow. Figure 5 represents the radial distance separating the column wall and the gas–liquid interface, along the longitudinal axis (the origin is at the bubble nose).

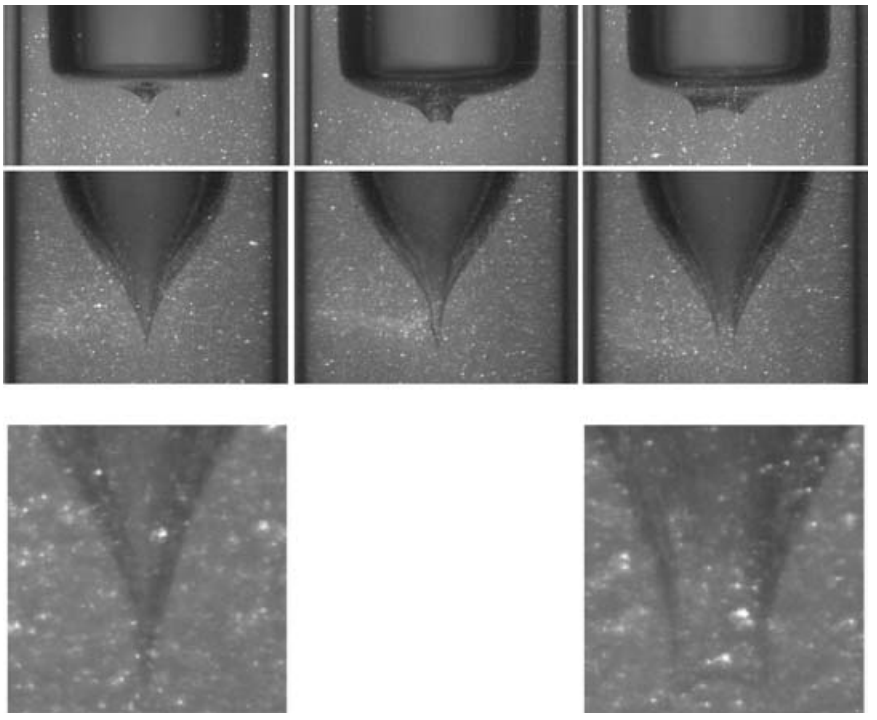

FIGURE 6. Shape of Taylor bubble trailing edges for 0.8 wt% CMC (top), 1.0 wt% CMC (centre) and zoom of the 1.0 wt% cusp (bottom).

The Taylor bubble nose is characterized by a prolate spheroid leading edge, which does not change significantly with the fluid properties, at least in the experimental conditions studied. The thickness of the falling liquid film around the bubble decreases with distance from the nose, until it reaches a constant value at around $z = 1.6D$ for 1.0 wt% and $z = 1.8D$ for 0.8 wt%. From there on, the film thickness remains constant, during a distance that depends on the bubble volume, until the trailing edge. The stabilized film thickness depends on the fluid viscosity and increases with increasing values of this rheological property. Until this point, the bubble shape is similar to those observed in Newtonian solutions.

The trailing edge is the zone of the Taylor bubble which most depends on the fluid properties. For highly viscous CMC solutions, the trailing edge is neither flat nor concave, as it is in Newtonian fluids and in non-Newtonian fluids with lower viscosities. For the 1.0 wt% CMC solution, the shape of the trailing edge is a two-dimensional cusp, similar to that described by Hassager (1979) and by other authors, as referred to by Liu *et al.* (1995). The two-dimensional cusp has no constant orientation, since it is possible to see it in different positions on consecutive images of the same bubble. This behaviour indicates a rotational movement of the cusp, similar to the one of an air core in a sink flow of a viscoelastic liquid. For the 0.8 wt% CMC solution, the images suggest a small axial oscillatory movement of the cusp edge, more precisely, a continuous expansion and contraction of the trailing edge. Different examples of the cusp edge observed in the experiments are shown in figure 6.

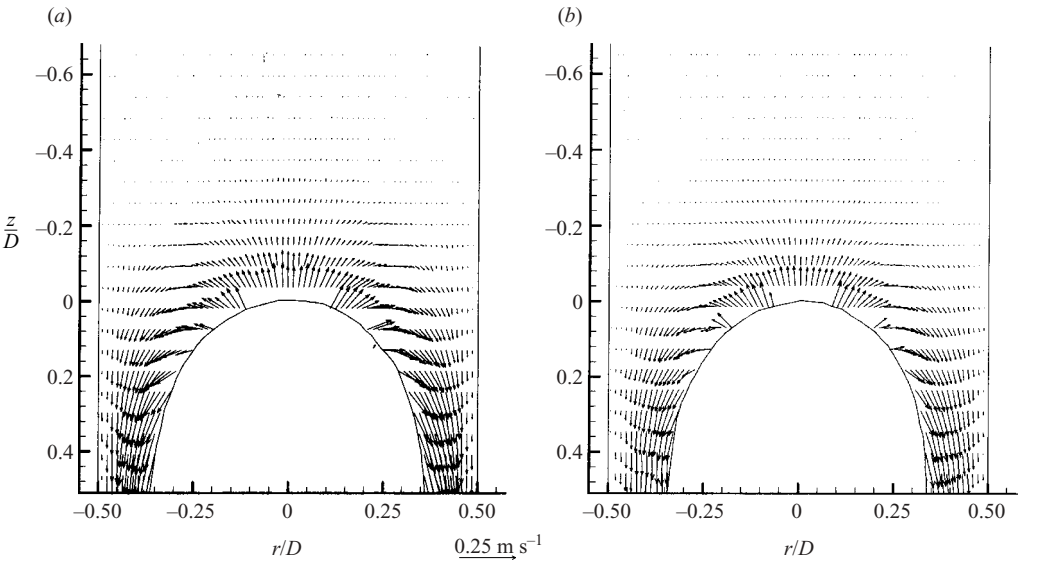


FIGURE 7. Flow field in the liquid around the Taylor bubble nose. (*a*) 0.8 wt% CMC; (*b*) 1.0 wt% CMC.

### 4.2. *Flow field*

The flow field around a Taylor bubble is described in the following sections. The vectors shown are the liquid velocity vectors, relative to a fixed reference frame, and although the resolution is of the order of $2 \times 10^{-4}$ m, some of them were not represented for better graphic visualization.

#### 4.2.1. *Nose*

The liquid in front of the bubble nose is pushed by the gas slug, so as to accomplish an upward movement. In the vicinity of the bubble, the radial velocity component increases towards the pipe wall and the liquid starts a downward movement around the bubble. Figure 7 shows the flow fields around the Taylor bubble for the two solutions studied. The flow patterns are identical, differing only slightly in the velocity magnitude, owing to the different Taylor bubble velocity. In figure 8, the axial component of the liquid velocity is represented along $z = 0$ for the studied cases.

#### 4.2.2. *Liquid film*

The liquid flowing around the Taylor bubble forms a falling film, whose thickness decreases with increasing distance from the bubble nose, according to the Taylor bubble shape represented in figure 5. The decrease in the liquid film thickness causes an increase in the axial velocity component, owing to mass conservation, until a stabilized film of constant thickness is reached. The axial instantaneous velocity profiles in the liquid film are represented in figure 9 at different bubble nose distances.

In figure 10, the axial component of the velocity is plotted along the axial coordinate in a fixed radial position. From figures 9 and 10, it is possible to conclude that the velocity profiles are stabilized after $z = 1.6D$ for 1.0 wt% and $z = 1.8D$ for 0.8 wt% CMC solution.

The average stabilized velocity profiles are represented in figure 11. These profiles were obtained by averaging several profiles in the stabilized liquid film; around 170 profiles from a PIV image, times 3 PIV images per bubble, times 5 bubbles of identical

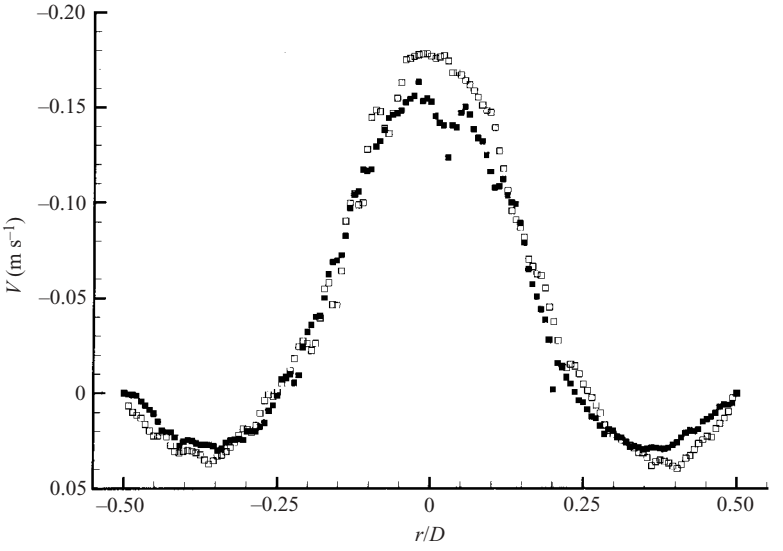


FIGURE 8. Axial component of liquid velocity along $z = 0$ for □, 0.8 wt% and ■, 1.0 wt% CMC solutions.

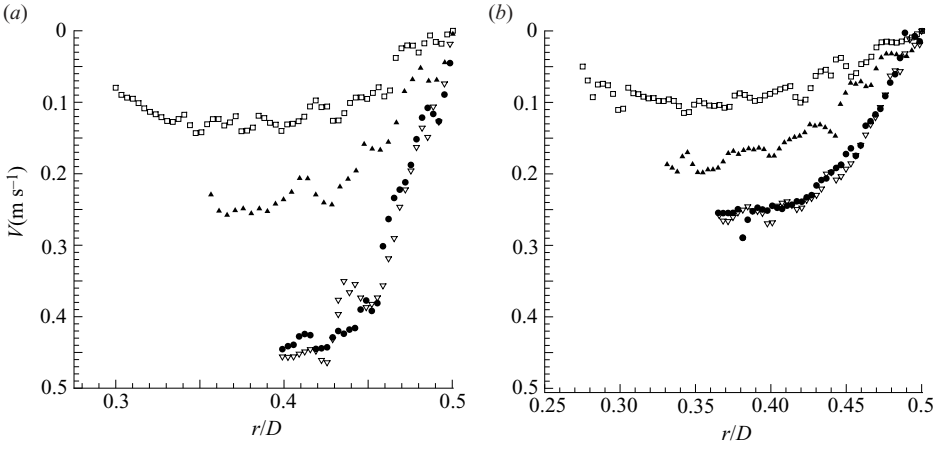


FIGURE 9. Axial component of velocity in the liquid film at different distances from the bubble nose. (*a*) 0.8 wt% CMC; (*b*) 1.0 wt% CMC. □, $z = 0.2D$; ▲, $0.4D$; ▽, $1.6D$; ●, $5.0D$.

volume. The average axial component of the velocity is higher in the 0.8 wt% CMC solution, which is in accordance with an expected higher flow rate due to a higher Taylor bubble velocity and a thinner liquid film. The maximum velocity in the liquid film is at the gas–liquid interface, as expected, since the shear stress there is almost zero (very low viscosity of the gas). The normal stresses have no effect on the profile since the flow is stabilized in the axial direction.

### 4.2.3. *Taylor bubble wake*

The wake is the region where the differences from the flow around Taylor bubbles rising in Newtonian liquids are more evident. As mentioned in § 4.1, the trailing

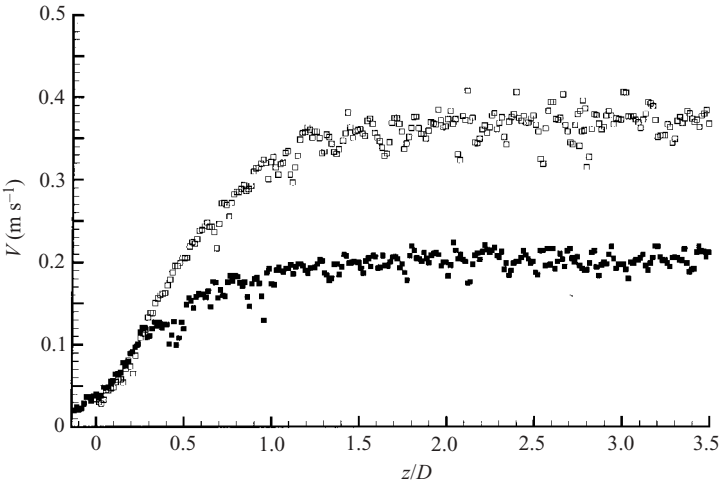


FIGURE 10. Axial component of velocity in the liquid film at $r = 0.45D$ between $z = 0D$ and $z = 3.5D$. □, 0.8 wt% CMC; ■, 1.0 wt% CMC.

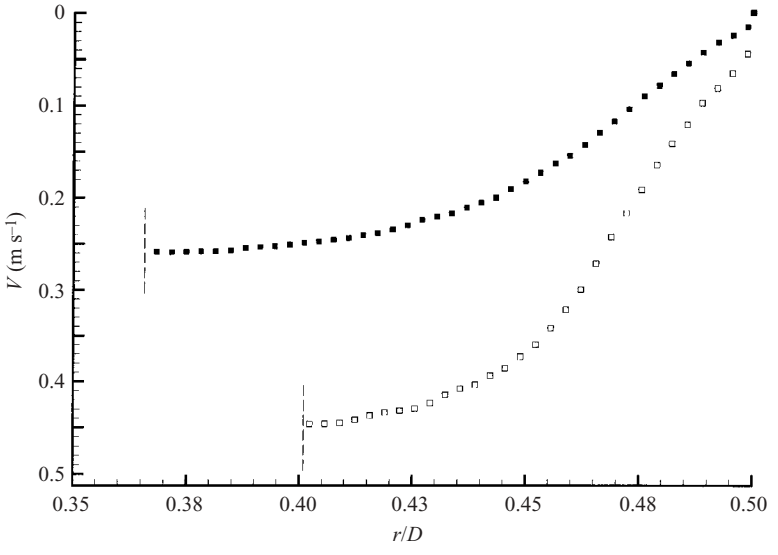


FIGURE 11. Average stabilized liquid film profiles for 0.8 wt% and 1.0 wt% CMC solutions. □, 0.8 wt% CMC; ■, 1.0 wt% CMC; - - -, bubble interface.

edge of a bubble rising in a 0.8 wt% CMC solution is oscillating, expanding and contracting continuously. The flow around a contracted edge and around a totally expanded edge is represented in figure 12. For a bubble rising in a 1.0 wt% CMC solution, the trailing edge is two-dimensional and has a rotational movement. The flow in two perpendicular planes is represented in figure 13. In figure 13(*a*), the wider dimension of the cusp is perpendicular to the laser sheet plane, i.e. to the paper plane, while in figure 13(*b*), the wider dimension of the cusp is now in the laser sheet plane. The shadowgraph is a two-dimensional projection of the bubble shape and so the projection in the paper plane of the width of the two-dimensional cusp in rotation at a constant velocity must be random, which corresponds to a uniform distribution in a

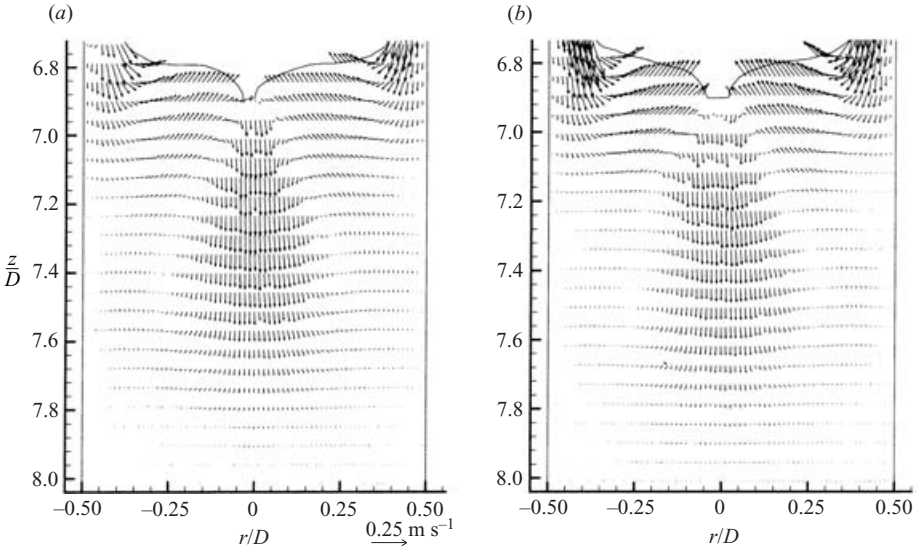


FIGURE 12. Flow field in the wake of a Taylor bubble rising in 0.8 wt% CMC solution.

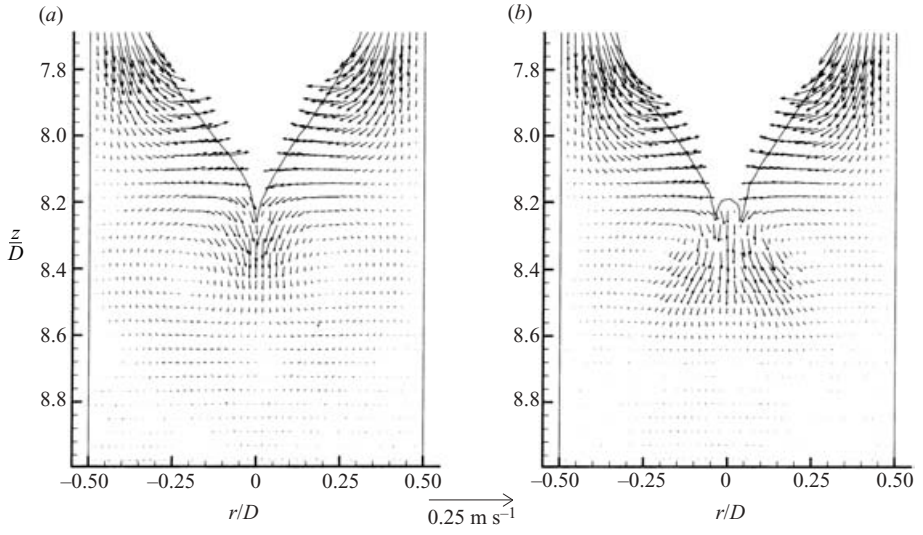


FIGURE 13. Flow field in the wake of a Taylor bubble rising in 1.0 wt% CMC solution.

large number of samples. A considerable number of images of the cusp in the 1.0 wt% CMC solution were analysed (about 120) and a quasi-uniform distribution was found (6 classes were considered between the minimum, 1 pixel, and the maximum value, 60 pixels – about $2.6 \times 10^{-3}$ m). This distribution suggests constant dimensions of the cusp and a constant rotational velocity. According to the images, the rotation frequency is very high, at least higher than the frequency of the CCD camera used in this visualization study (25 Hz). It was impossible to detect the direction of the rotation from the images.

In both solutions, the fluid coming from the liquid film suffers a sudden deceleration when reaching the bottom of the Taylor bubble and acquires a radial velocity

towards the centre of the column. It should be kept in mind that the vectors are relative to a fixed reference frame and the Taylor bubble is moving upward. The velocity vectors might give the impression that the fluid is entering into the gas bubble, but it is just moving to the space occupied by the Taylor bubble the instant before.

The radial displacement of the fluid towards the centre of the column, induces, by momentum diffusion, movement in the fluid that is immediately below. This fluid initiates a rotational displacement, going down in the centre of the column and up far from the centre. The downward displacement of the fluid does not appear in the wake of Taylor bubbles rising in Newtonian fluids and is the reason why this wake is called a negative wake. While the velocity in the central downward fluid reaches 90% of the Taylor bubble velocity for 0.8 wt% CMC and 45% of the bubble velocity for 1.0 wt%, the maximum upward velocities in the circulating region, far from the tube axis, reach only 10% and 6% of the bubble velocity, respectively. The higher velocity in the centre of the column is due to mass conservation across a cross-sectional area.

In figures 12(*a*) and 12(*b*), 0.8 wt% CMC solution, the main difference in the flow pattern is the velocity magnitude close to the bubble interface. The upward liquid velocity is lower when the edge is moving down, contracted edge initiating the expansion, as seems to be the case in figure 12(*a*). In figure 12(*b*), the trailing edge is totally expanded and the upward velocity is higher. This behaviour will be seen better in a moving reference frame (figure 18).

In figures 13(*a*) and 13(*b*), 1.0 wt% CMC solution, the main difference is the provenance of the liquid that is going downwards in the centre below the bubble trailing edge. In figure 13(*a*), the wider dimension of the cusp is perpendicular to the laser sheet plane (paper plane) and all the liquid that is going downward in the centre comes from this plane. In figure 13(*b*), the cusp wider dimension is now in the laser sheet plane and the liquid that is going downward in the centre comes from other planes inclusive of the plane represented in figure 13(*a*). Therefore, in the centre below the cusp, the vectors represented in figure 13(*b*) should have a velocity component normal to the laser sheet plane, i.e. the flow in the wake region should be asymmetric (three-dimensional flow).

From these figures, it can be concluded that the asymmetric shape of the trailing edge for the 1.0 wt% CMC solution is responsible for an asymmetric flow in the wake region (three-dimensional flow). Taking into account the small dimension of the cusp, the magnitude of these asymmetries must be quantified.

Figure 14 shows the vertical velocity component along an horizontal line at 0.3$D$ downward of the trailing edges represented in figures 12($a, b$) and 13($a, b$). The downward velocity in the centre is much higher in the 0.8 wt% solution, in accordance with the lower viscosity of the fluid and higher liquid velocity in the stabilized liquid film.

The flow rate in the wake was computed integrating in the cross-sectional area the velocity profile at 0.3$D$ from the trailing edge; this procedure was repeated taking different images of a bubble and different bubbles. The flow rate should be zero according to mass conservation.

For the 0.8 wt% solution, the values of the flow rate are very low, around zero, and no consistent tendency (lower or higher than zero) was found. For the 1.0 wt% solution, there is a tendency for the flow rate to be negative, fluid flowing away from the paper plane, in the case represented in figure 13(*a*) and positive, fluid flowing into the paper plane, in the case represented in figure 13(*b*). This behaviour supports

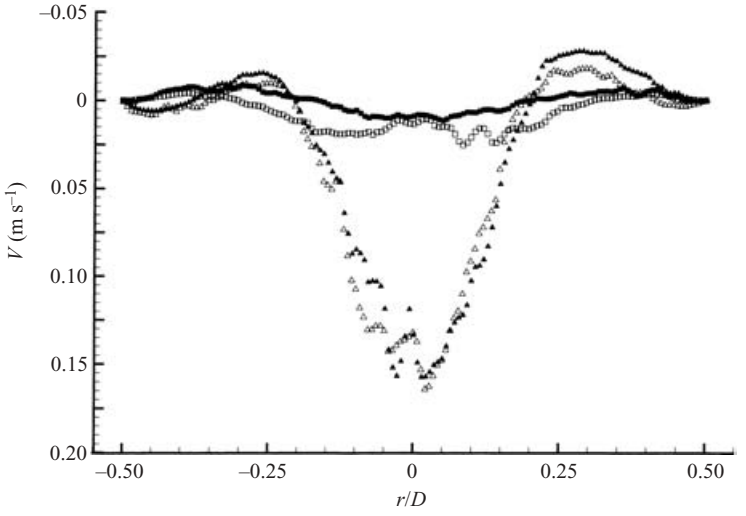


FIGURE 14. Vertical component of velocity along a horizontal line at 0.30$D$ downward of the trailing cusp, from figures 12 and 13. ▲, 0.8 wt% CMC; △, 0.8 wt% CMC; ■, 1.0 wt% CMC; □, 1.0 wt% CMC.

the flow description presented above. The magnitude of the integrated flow rates is, however, low, from $2 \times 10^{-7}$ to $2 \times 10^{-6}\,\mathrm{m^3\,s^{-1}}$. To make accurate conclusions, this order of magnitude must be compared with the magnitude of the error associated to the flow rate. This will be done in § 4.3.

Although the circulatory movement induced in the wake of the Taylor bubble has a very low velocity magnitude and a short time duration, it is possible to see, by increasing the time between the PIV frames to the order of milliseconds, that this circulatory movement induces other similar movements in the downward adjacent fluid, alternating the rotation direction. An example of this behaviour, is represented in figure 15.

It is worth remembering that the velocity magnitude in the second rotational movement is now of the order of 2% of the Taylor bubble velocity, which means that this movement is not perceptible in a reference frame moving with the Taylor bubble, as will be shown in the next section. These second rotational movements are visible mainly in the 1.0 wt% CMC solution and when the cusp wider dimension is perpendicular to the paper plane; they are not as visible in the 0.8 wt% solution.

The shear rates were computed from the flow field and the local instantaneous viscosity determined from the rheological properties. In figure 16, the local viscosity fields are represented, considering that the viscosity is only a function of the instantaneous shear rate, neglecting the relaxation times. The local shear rate was computed according to

$$\dot{\gamma} = \sqrt{\tfrac{1}{2} \sum_i \sum_j \dot{\gamma}_{ij} \dot{\gamma}_{ji}}, \tag{4.2}$$

where $\dot{\gamma}_{i,j} = \partial V_i / \partial x_j$. From figure 16, it is possible to see that the viscosity increases one order of magnitude, when moving from the liquid film to the wake and that in the wake (central zone), the viscosity is lower than in the liquid below.

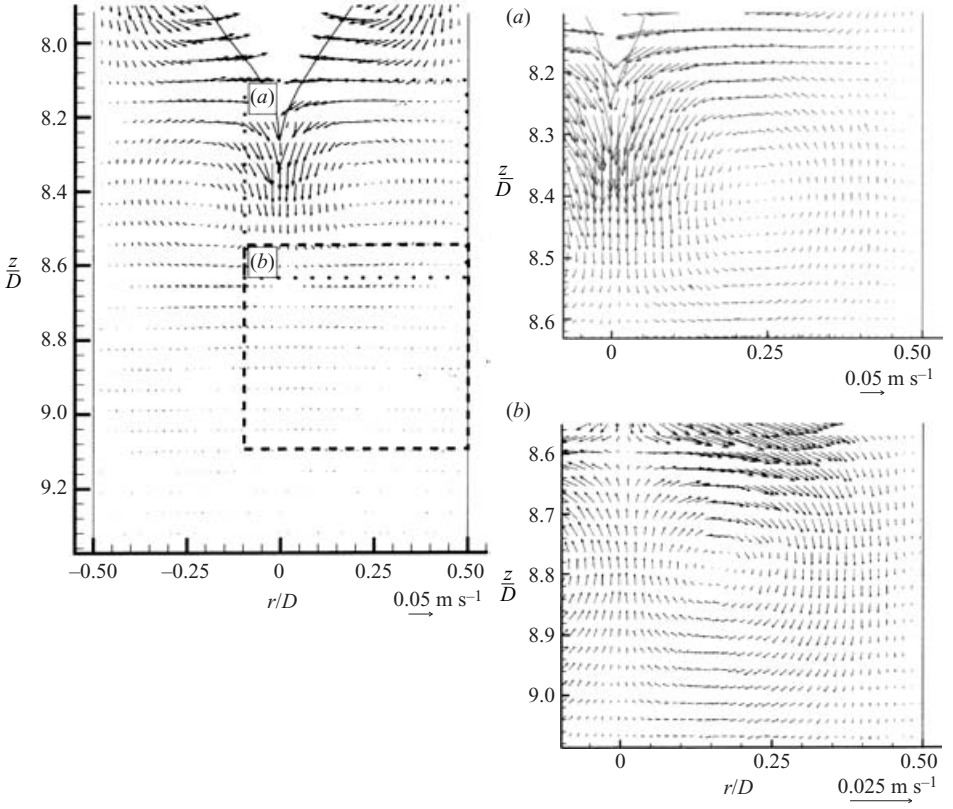


FIGURE 15. Circulatory movements of the fluid in the wake of a Taylor bubble rising in 1.0 wt% CMC solution.

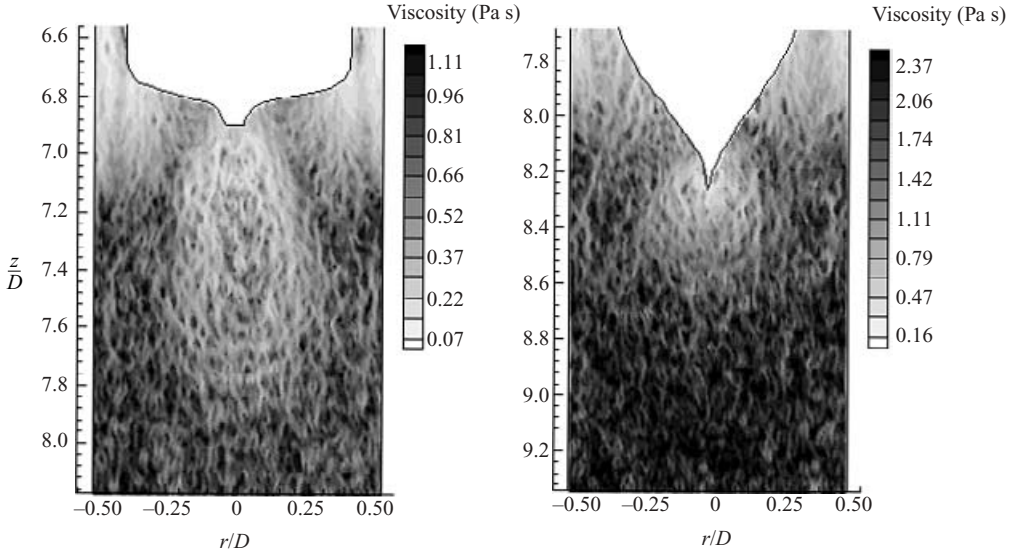


FIGURE 16. Viscosity field in the wake of Taylor bubbles rising in 0.8 and 1.0 wt% CMC solutions.

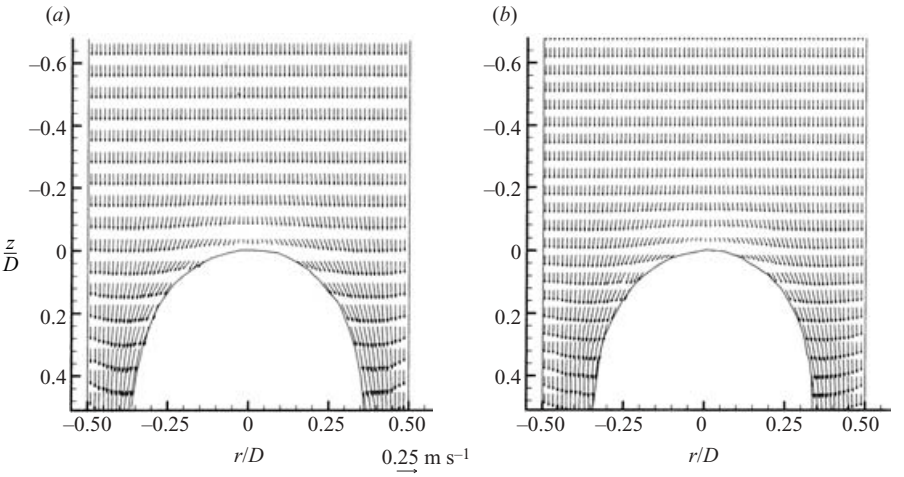


FIGURE 17. Flow field around the nose of Taylor bubbles rising in (*a*) 0.8 wt% and (*b*) 1.0 wt% CMC solutions, in a reference frame moving with the gas bubble.

### 4.3. *Moving reference frame*

In the flow fields represented in § 4.2, the velocities were relative to a fixed reference frame. The flow fields near the nose of the Taylor bubbles are represented in figure 17, relative to a reference frame moving with the gas bubble. It can be seen that the liquid goes around the bubble and the vectors are now tangent to the gas–liquid interface. There are a few exceptions owing to inaccuracies in the processing of interrogation windows that partially contain the gas bubble interface.

The flow fields in the wake of the Taylor bubbles, relative to a reference frame moving with the bubble are represented in figures 18 and 19 . The rotational fluid movements in the wake of the bubbles are no longer perceptible.

For the 0.8 wt% CMC solution (figure 18), it is possible to see the axial movement of the cusp. In figure 18(*b*), the vectors are tangent to the bubble interface, meaning that the cusp is moving at the velocity of the bubble; the cusp is fully expanded. In figure 18(*a*), there is a normal outward velocity component relative to the bubble interface, meaning that the trailing edge is moving down, relative to the bubble; the contracted cusp is expanding, thrusting the fluid forward.

In the 1.0 wt% CMC solution (figure 19), the vectors are tangent to the bubble interface in both cases, as would be expected once no axial movement was perceptible in the cusp.

In the reference frame moving with the bubble, the liquid flow rate in any cross-section of the column must be the same. The liquid flow rate in a cross-section ahead of the Taylor bubble is given by

$$Q_{front} = \int_0^R (U_{exp}(r) - U_{gb}) 2\pi r \, \mathrm{d}r, \tag{4.3}$$

where $U_{exp}(r)$ is the velocity of the liquid in front of the Taylor bubble nose, induced by the gas bubble expansion and $U_{gb}$ is the velocity of the gas bubble. Both velocities are negative, according to the coordinate axis chosen, and both are relative to a fixed reference frame. The pipe radius is represented by $R$.

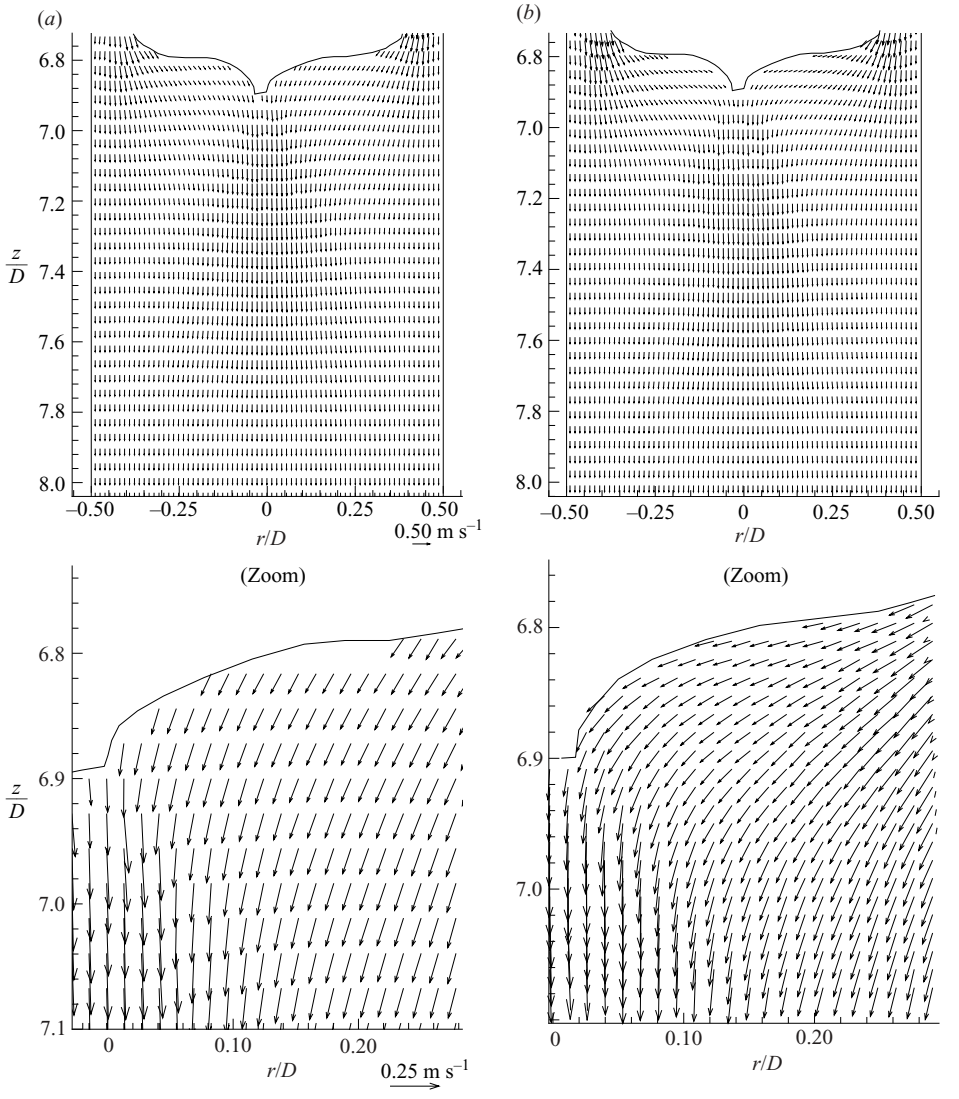


FIGURE 18. Flow field in the wake of Taylor bubbles rising in 0.8 wt% CMC solution, in a reference frame moving with the gas bubble.

The flow rate around the Taylor bubble through a cross-section at a given position $z$ is given by

$$Q_z = \int_{R-\delta(z)}^{R} (U_{film}(r) - U_{gb}) 2\pi r \, \mathrm{d}r, \tag{4.4}$$

where $\delta(z)$ is the liquid film thickness at the axial position $z$.

The flow rate ahead of the bubble was compared with the flow rate at different axial positions, $z$, in the liquid film. The percentage deviation of $Q_z$ relative to $Q_{front}$ for the studied cases is represented in figure 20. The deviation between the flow rate in front of the bubble and the flow rate at different axial positions in the liquid film along the bubble is always less than 2.5% for 0.8 wt% and 1.0% for 1.0 wt%.

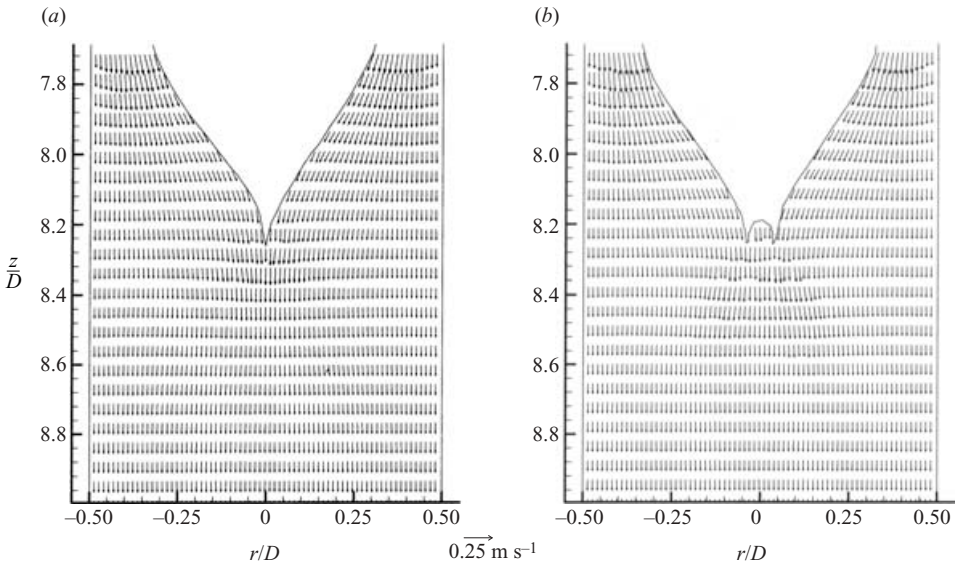


FIGURE 19. Flow field in the wakes of Taylor bubbles rising in 1.0 wt% CMC solution, in a reference frame moving with the gas bubble.

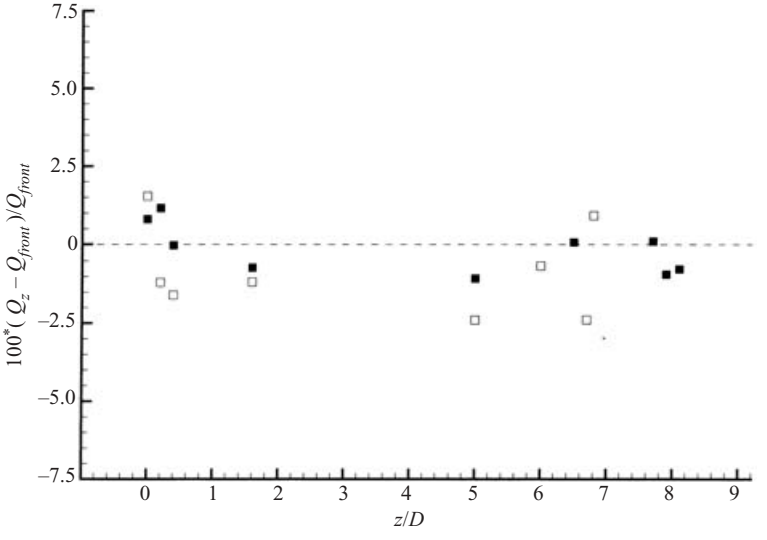


FIGURE 20. Percentage deviation of $Q_z$ relative to $Q_{front}$. □, 0.8 wt% CMC; ■, 1.0 wt% CMC.

The liquid flow rate flowing around the slug for 0.8 wt% in a moving reference frame is $1.45 \times 10^{-4}$ m$^3$ s$^{-1}$ and for 1.0 wt% is $1.28 \times 10^{-4}$ m$^3$ s$^{-1}$. Hence, the flow rates experimentally obtained at $0.3D$ from the bubble edge for 1.0 wt% (§ 4.2.3) have a maximum deviation of $\pm 1.5\%$ from the axisymmetric flow rate. This value is low, slightly higher than the estimated error, suggesting small asymmetries in the wake flow owing to the two-dimensional cusp in rotation.

## 5. Conclusions

The flow around Taylor bubbles rising in 0.8 and 1.0 wt% CMC solutions was studied applying particle image velocimetry and shadowgraphy simultaneously.

(i) Bubble nose shapes are similar to those found in Newtonian liquids, but trailing edges have different configurations: a two-dimensional cusp in rotation for 1.0 wt%, and a cusp with axial oscillations for 0.8 wt%.

(ii) Negative wakes, with fluid going in the opposite direction to the bubble, were found. Secondary rotational liquid movements far from the bubble were also found for 1.0 wt%.

(iii) The asymmetric shape of the trailing edge for 1.0 wt% is responsible for small asymmetries in the flow in the wake region (three-dimensional flow).

(iv) The edge oscillation found for 0.8 wt% does not induce any detectable non-axisymmetric flow in the wake.

(v) Viscosity field in the wake of the Taylor bubbles was determined and changes of one order of magnitude are observed.

(vi) Results were validated by mass flow balances at different axial positions along the liquid film.

The presented study and conclusions are essential for a future better understanding of the coalescence phenomena.

The authors acknowledge the financial support given by FCT, SFRH/BD/3389/2000 and the Von Karman Institut for the facility. This work was also supported, via CEFT, by POCTI (FEDER).

## REFERENCES

Acharya, A., Mashelkar, R. A. & Ulbrecht, J. 1977 Mechanics of bubble motion and deformation in non-Newtonian media. *Chem. Engng Sci.* **32**, 863–872.

Acharya, A. & Ulbrecht, J. J. 1978 Note on the influence of viscoelasticity on the coalescence rate of bubbles and drops. *AIChE J.* **24**, 348–351.

Astarita, G. & Apuzzo, G. 1965 Motion of gas bubbles in non-Newtonian liquids. *AIChE J.* **11**, 815–820.

Bugg, J. & Saad, G. A. 2002 The velocity field around a Taylor bubble rising in a stagnant viscous fluid: numerical and experimental results. *Intl J. Multiphase Flow* **28**, 791–803.

Campos, J. B. L. M. & Guedes de Carvalho, J. R. F. 1988 An experimental study of the wake of gas slugs rising in liquids. *J. Fluid Mech.* **196**, 27–37.

Carew, P. S., Thomas, N. H. & Johnson, A. B. 1995 A physical based correlation for the effects of power law rheology and inclination on slug bubble rise velocity. *Intl J. Multiphase Flow* **21**, 1091–1106.

De Kee, D., Chhabra, R. P. & Dajan, A. 1990 Motion and coalescence of gas bubbles in non-Newtonian polymer solutions. *J. Non-Newtonian Fluid Mech.* **37**, 1–18.

Funfschilling, D. & Li, H. Z. 2001 Flow of non-Newtonian fluids around bubbles: PIV measurements and birefringe visualisation. *Chem. Engng Sci.* **56**, 1137–1141.

Hassager, O. 1979 Negative wake behind bubbles in non-Newtonian liquids. *Nature* **279**, 402–403.

van Hout, R., Gulitski, A., Barnea, D. & Shemer, L. 2001 Experimental investigation of the velocity field induced by a Taylor bubble rising in stagnant water. *Intl J. Multiphase Flow* **28**, 579–596.

Leal, L. G., Skoog, J. & Acrivos, A. 1971 On the motion of gas bubbles in a viscoelastic liquid. *Can. J. Chem. Engng* **49**, 569–575.

Li, H. Z., Frank, X., Funfschilling, D. & Mouline, Y. 2001 Towards the understanding of bubble interactions and coalescence in non-Newtonian fluids: a cognitive approach. *Chem. Engng Sci.* **56**, 6419–6425.

Lindken, R. & Merzkirch, W. 2002 A novel PIV technique for measurements in multi-phase flows and its application to two-phase bubbly flows. *Exps. Fluids* **33**, 814–825.

Liu, Y. J., Liao, T. Y. & Joseph, D. D. 1995 A two-dimensional cusp at the trailing edge of an air bubble rising in a viscoelastic liquid. *J. Fluid Mech.* **304**, 321–342.

Moissis, R. & Griffith, P. 1962 Entrance effects in a two-phase slug flow. *Trans. ASME* C: *J. Heat Transfer*, **2**, 29–39.

Nogueira, S., Dias, I., Pinto, A. M. F. R. & Riethmuller, M. L. 2000 Liquid PIV measurements around a single gas slug rising through stagnant liquid in vertical pipes. In *Bound Volume of Selected Papers of the '10th Symposium on Laser Techniques Applied to Fluid Dynamics'*. Springer.

Nogueira, S., Sousa, R. G., Pinto, A. M. F. R., Riethmuller, M. L. & Campos, J. B. L. M. 2003 Simultaneous PIV and shadowgraphy in slug flow: a solution for optical problems. *Expts Fluids* **35**, 598–609.

Otten, L. & Fayed, A. S. 1976 Pressure drop and drag reduction in two-phase non-Newtonian slug flow. *Can. J. Chem. Engng* **54**, 111–114.

Pinto, A. M. F. R. & Campos, J. B. L. M. 1996 Coalescence of two gas slugs rising in a vertical column of liquid. *Chem. Engng Sci.* **51**, 45–54.

Polonsky, S., Barnea, D. & Shemer, L. 1998 Image processing procedure for analysing the motion of an elongated bubble rising in a vertical pipe. *8th Intl Symp. Flow Visualisation*, pp. 117.1–117.10.

Rosehart, R. G., Rhodes, E. & Scott, D. S. 1975 Studies of gas–liquid (non-Newtonian) slug flow: void fraction meter, void fraction and slug characteristics. *Chem. Engng J.* **10**, 57–64.

Scarano, F. & Riethmuller, M. L. 1999 Iterative multigrid approach in PIV image processing with discrete window offset. *Expts Fluids* **26**, 513–523.

Taitel, Y., Barnea, D. & Dukler, A. 1980 Modelling flow pattern transitions for steady upward gas–liquid flow in vertical tubes. *AIChE J.* **3**, 345–354.

Terasaka, K. & Tsuge, H. 2003 Gas holdup for slug bubble flow of viscous liquids having a yield stress in bubble columns. *Chem. Engng Sci.* **58**, 513–517.

White, E. T. & Beardmore, R. H. 1962 The velocity of rise of single cylindrical air bubbles through liquids contained in vertical tubes. *Chem. Engng Sci.* **17**, 351–361.